RSC Advances

PAPER

View Article Online
View Journal | View Issue

Cite this: *RSC Adv.*, 2026, **16**, 10363

Preparation and performance evaluation of expanded vermiculite-based phase change materials for building thermal insulation and energy saving

Chaoqun Fan, [a] Hanning Zhang,[a] Jiaxing Gao,[a] Haiming Yang[b] and Xifeng Lv*[a]

To meet the demand for building envelope materials with efficient heat storage and release capabilities in the harsh climate of Northwest China, this study reports the development of a novel ternary composite phase change material (CEV@SiC). The material was prepared by vacuum impregnation, encapsulating calcium chloride hexahydrate into highly porous expanded vermiculite and further incorporating silicon carbide nanoparticles as thermal conductivity enhancers. Thermal analysis showed that the sample with 5% SiC doping exhibited the highest enthalpy of fusion (90.3 J g^{-1}) and retained 95% of its enthalpy after 100 thermal cycles, demonstrating excellent cycling stability. A microscale heat transfer model of phase change mortar was established through simulation, and test modules incorporating CEV@SiC as a partial replacement for aggregate in cement mortar were constructed. Compared with ordinary modules, the CEV@SiC-modified modules reduced the indoor peak temperature by 2.04 °C and delayed the occurrence of the peak temperature by 1 h, confirming their significant energy-saving and temperature-regulation potential. This study provides crucial insights into component design and process optimization for developing high-performance phase change materials tailored for building envelopes in Northwest China. The developed material effectively fulfils the dual requirements of high thermal storage density and rapid thermal response under the region's unique climatic conditions.

Received 3rd December 2025
Accepted 6th February 2026

DOI: 10.1039/d5ra09349j

rsc.li/rsc-advances

1. Introduction

The continental climate[1] of Northwest China—characterized by harsh winters, scorching summers, sharp diurnal temperature swings, low humidity, and intense solar radiation—poses significant challenges for building insulation[2] and dynamic thermal management.[3] These conditions exacerbate building energy consumption, making efficient thermal regulation a critical concern for sustainable development in such regions.[4] Conventional building materials[5] often struggle under these extremes. Their limited thermal mass and heat storage capacity lead to pronounced indoor temperature fluctuations, increasing the reliance on active heating and cooling systems and, consequently, overall energy use.[6]

To simultaneously achieve energy efficiency[7] and indoor comfort, integrating advanced functional materials into building envelopes has become a key research focus.[8] In this context, improving building energy performance through optimized design and material innovation is essential. Studies have explored various mechanisms, such as optimizing temperature setpoints under different envelopes for cooling energy savings,[9] and assessing the impact of facade-integrated photovoltaic retrofits on carbon emissions in residential buildings.[10] Phase change materials (PCMs),[11] particularly hydrated salts[12] such as calcium chloride hexahydrate ($CaCl_2 \cdot 6H_2O$), are regarded as a highly promising technology for enhancing thermal energy storage capacity. They offer suitable phase transition temperatures, high latent heat,[13] low cost, and abundant availability.[14] However, their widespread application is hindered by inherent drawbacks like liquid leakage, supercooling, and phase separation,[15–17] which compromise long-term stability and reliability.[18]

A common strategy to overcome these issues is to encapsulate hydrated salts within porous matrices, such as expanded perlite or expanded vermiculite (EV).[19–21] These shape-stabilized composites prevent leakage but introduce a new challenge: their thermal conductivity[22] is often significantly lower than that of conventional foam insulation materials.[23] For instance, while polystyrene foam exhibits a conductivity of about 0.03–0.04 W m^{-1} K^{-1}, typical salt/porous matrix composites report values around 0.178 W m^{-1} K^{-1}. This low conductivity, while providing some insulation, severely impedes the rates of heat storage and release,[24] which is critical for responsive thermal management. Research into enhancing the functional

[a]College of Chemistry and Chemical Engineering, Tarim University, Alar, Xinjiang, 843300, China. E-mail: lvning7431@163.com
[b]Xinjiang Xingye New Building Materials Co., Ltd., Alar, Xinjiang, 843300, China

properties of composite materials, such as improving the thermal stability and enthalpy of wood-based composites *via in situ* polymerization of graphene oxide-modified PCM microcapsules,[25] highlights the ongoing efforts to refine PCM performance. Similarly, studies on optimizing other material systems, like the design of cylindrical thermal classifiers based on transformation thermodynamics[26] or the multi-objective optimization of thermoelectric modules,[27] underscore the importance of tailored thermal transport and energy conversion in advanced material design.

Under the sharp diurnal temperature fluctuations typical of Northwest China, the low thermal conductivity of standard PCM composites restricts their ability to rapidly absorb excess heat during the day and release it at night, thereby diminishing their effectiveness in dynamic thermal regulation.[28] Therefore, enhancing the thermal conductivity of shape-stabilized PCMs without compromising their storage density, shape stability, or cost-effectiveness is a crucial research direction. Innovations in other cementitious and ceramic composites, such as developing novel green lithium slag expansion agents for mortar,[29] utilizing carrier-embedded microbial calcium carbonate in cement mortars,[30] or understanding the mechanisms behind microstructure regulation in foamed ceramics,[31] demonstrate the broad potential of composite material engineering for achieving enhanced and multifunctional properties.

To address this specific conductivity challenge, this study innovatively introduces high-thermal-conductivity silicon carbide (SiC) into a calcium chloride hexahydrate/expanded vermiculite composite system as a thermal-conductivity-enhancing phase. This approach aligns with the broader need for intelligent energy management in buildings, which can be informed by strategies considering factors like price fluctuations in HVAC system operation.[32] By precisely controlling the SiC content, we aim to significantly improve the thermal transport rate of the composite while maintaining effective PCM encapsulation, high thermal storage density, and adequate insulation properties. This design targets a substantial enhancement in the dynamic heat storage and release performance of the composite under frequent and large temperature swings. The development of such a multifunctional composite, which synergistically combines high energy density, rapid thermal response, and good stability, holds significant scientific value and promising practical prospects for energy-efficient buildings in extreme climates.

2. Materials and methods

2.1 Reagents and instruments

Anhydrous calcium chloride ($CaCl_2$) and strontium chloride hexahydrate ($SrCl_2 \cdot 6H_2O$, AR grade) were purchased from Macklin Biochemical Co., Ltd. (Shanghai, China). Vermiculite was supplied by Xinlong Vermiculite Co., Ltd. (Yuli, Xinjiang, China). Silicon carbide (SiC, AR grade) was obtained from Zhiyuan Chemical Reagent Co., Ltd. (Tianjin, China). Cement mortar was provided by Zhejiang Construction New Building Materials Group Co., Ltd.

2.2 Sample preparation

Firstly, 10.14 g of anhydrous $CaCl_2$ was dissolved in 9.86 g of deionized water, followed by the addition of 0.40 g of $SrCl_2 \cdot 6H_2O$. The mixture was stirred in a water bath at 50 °C for 1 h and subsequently cooled to crystallize $CaCl_2 \cdot 6H_2O$. Vermiculite particles (2 mm in diameter) were dried and expanded using a 1200 W microwave treatment to obtain expanded vermiculite (EV). A vacuum impregnation method was then employed to incorporate molten $CaCl_2 \cdot 6H_2O$ into EV at mass ratios of 40%, 50%, and 60% under conditions of 50 °C and 85 kPa for 30 min, followed by drying for 5 h to yield $CaCl_2 \cdot 6H_2O$/EV (CEV) composite phase change materials (PCMs). Furthermore, nano-SiC particles were incorporated into the molten $CaCl_2 \cdot 6H_2O$ at 1, 5, 9, and 13 wt% loadings, and the above impregnation process was repeated to prepare $CaCl_2 \cdot 6H_2O$/EV@SiC (CEV@SiC) ternary composites. All prepared samples were finally stored under refrigeration. The preparation procedure is schematically illustrated in Fig. 1.

2.3 Characterization

The morphology and elemental composition of the samples were characterized using scanning electron microscopy coupled with energy-dispersive X-ray spectroscopy (SEM-EDS, ZEISS Gemini 300/Smartedx). The chemical functional groups and component compatibility of the composite were investigated by Fourier transform infrared spectroscopy (FTIR, Thermo Fisher Nicolet 6700) over a wavenumber range of 4000–400 cm^{-1}. The crystal structure was analyzed by X-ray diffraction (XRD, Bruker D8-ADVANCE) with 2θ scanned from 10° to 90° at a rate of 5° min^{-1}. The phase transition temperatures and enthalpies were determined using differential scanning calorimetry (DSC, Mettler DSC1) under a nitrogen atmosphere, with a heating rate of 5 °C min^{-1} between 10 and 60 °C. Thermal conductivity was measured *via* the steady-state heat flow method using a DRE-III instrument. Thermal stability was evaluated by thermogravimetric analysis (TGA, Mettler TGA/DSC3+) from 10 to 600 °C at a heating rate of 5 °C min^{-1}. Leakage behavior was assessed by heating the samples at 60 °C for 1 h, with regular photographic and infrared monitoring. A mesoscopic heat transfer model was

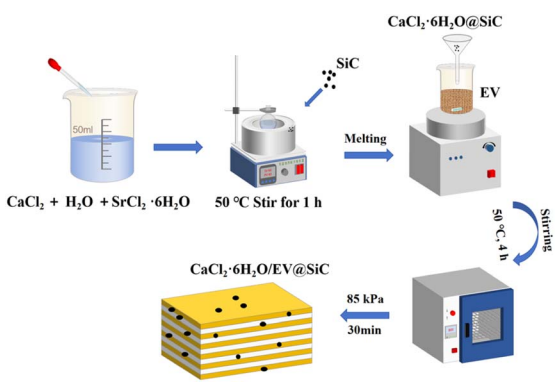

Fig. 1 Schematic diagram of the preparation process for $CaCl_2 \cdot 6H_2O$/expanded vermiculite@SiC (CEV@SiC) composite phase change material.

established using COMSOL Multiphysics, and the practical temperature regulation performance was evaluated by incorporating the composite into a cement plaster model room (300 mm × 300 mm × 300 mm) for outdoor testing.

3. Results and discussion

3.1 Maximum absorption capacity of composite phase change materials

To determine the maximum uptake (loading) capacity of expanded vermiculite (EV) for $CaCl_2 \cdot 6H_2O$, $CaCl_2 \cdot 6H_2O$/EV (CEV) composites with three different mass fractions were placed on separate filter papers. The papers were kept in an oven at 50 °C for 1 h to ensure complete melting of the PCM. After removal, the samples were lifted off the papers, and the filter papers were carefully inspected for any wetting indicative of leakage. Representative results are shown in Fig. 2.

The experimental results indicate that when the mass fraction of $CaCl_2 \cdot 6H_2O$ in the CEV composite is 40% or 50% (Fig. 2a and b), the material's adsorption capacity does not reach saturation. No liquid residues were detected on the filter paper after heating, demonstrating that the solute is fully retained within the vermiculite pores. However, increasing the $CaCl_2 \cdot 6H_2O$ content to 60% led to liquid seepage on the filter surface (Fig. 2c), suggesting that the adsorption sites of EV had reached saturation and the excess solute exceeded the structural carrying capacity, causing leakage. Overall, the maximum adsorption capacity of the CEV composite for $CaCl_2 \cdot 6H_2O$ is 50%, at which the material exhibits optimal adsorption stability and solute encapsulation efficiency during the thermal phase change process.

3.2 Morphology and chemical compatibility of CEV and CEV@5% SiC composite PCM

Fig. 3a displays the typical layered porous structure of expanded vermiculite (EV), which features uniform interlayer spacing and continuous pore distribution, providing ideal adsorption sites and thermal energy storage space for phase change materials. Fig. 3b illustrates the microstructure of the CEV composite after impregnation with 50 wt% calcium chloride hexahydrate ($CaCl_2 \cdot 6H_2O$). The molten salt, driven by capillary forces, uniformly fills the pores of vermiculite, forming a dense composite interface without significant phase separation or salt leakage, indicating that the vacuum impregnation method effectively achieves efficient encapsulation of the phase change material Fig. 3c corresponds to the CEV@5% SiC ternary composite, in which SiC nanoparticles (bright black dots) are uniformly dispersed on the surface and within the pores of vermiculite without agglomeration, while calcium chloride hexahydrate remains fully loaded. The introduction of silicon carbide does not disrupt the porous network of expanded vermiculite but instead enhances interfacial heat conduction pathways, improving thermal conductivity. This is consistent with the differential scanning calorimetry (DSC) results discussed later—the melting enthalpy of this composite material increases ($\Delta H_m = 90.3$ J g^{-1}).

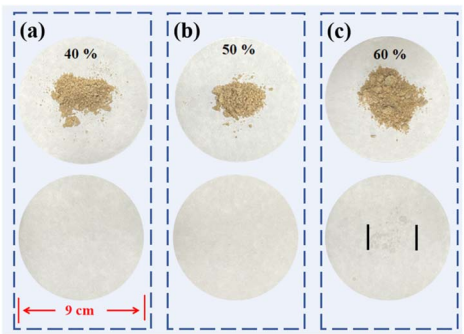

Fig. 2 Leakage behavior and maximum absorption capacity of CEV composite phase change materials with different $CaCl_2 \cdot 6H_2O$ mass fractions ((a) 40 wt%; (b) 50 wt%; (c) 60 wt%).

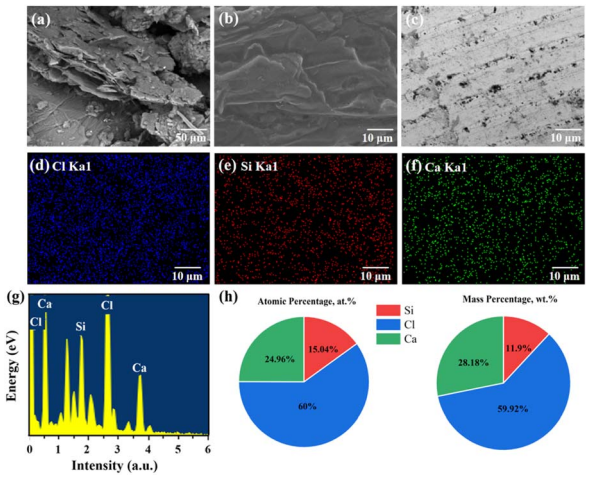

Fig. 3 (a) SEM images of (a) EV, (b) CEV, and (c) CEV@5% SiC. (d–f) Elemental mapping images of (d) Cl, (e) Si, and (f) Ca corresponding to the area in (c). (g) EDS survey spectrum and (h) the corresponding elemental atomic and weight percentages derived from the area shown in (c).

Energy-dispersive X-ray spectroscopy analysis of the scanning electron microscopy image Fig. 3(c) (Fig. 3d–f) reveals the presence of characteristic elements in the CEV@5% SiC composite: calcium (Ca, 28.18 wt%), chlorine (Cl, 59.92 wt%), and silicon (Si, 11.90 wt%). Detailed data are summarized in Fig. 3(g) and (h). The atomic ratio of calcium to chlorine is approximately 1 : 2.4 (the theoretical atomic ratio for calcium chloride is 1 : 2), confirming the successful loading of calcium chloride hexahydrate into the vermiculite matrix. The atomic percentage of silicon (15.04 wt%) is significantly higher than its mass percentage (11.90 wt%), which is attributed to the contribution of low-density silicon carbide nanoparticles (density $\rho = 3.21$ g cm^{-3}). After deducting the silicon inherently present in vermiculite (approximately 8.4 wt%), the additional silicon content (approximately 3.5 wt%) matches the designed 5% silicon carbide doping level exactly, further confirming the successful construction of the CEV@5% SiC ternary composite structure.

Fig. 4a shows the FT-IR spectrum of the CEV@5% SiC composite. The broad peak at 3435.44 cm^{-1} corresponds to O–H

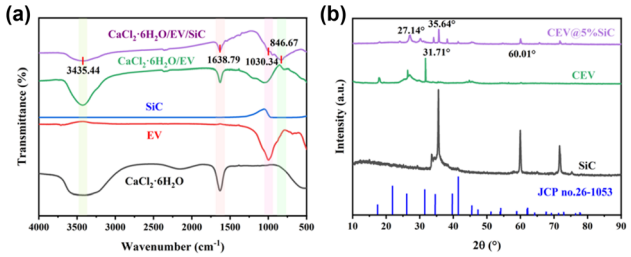

Fig. 4 (a) FTIR and (b) XRD spectra of $CaCl_2·6H_2O$, SiC, CEV, and CEV@5% SiC.

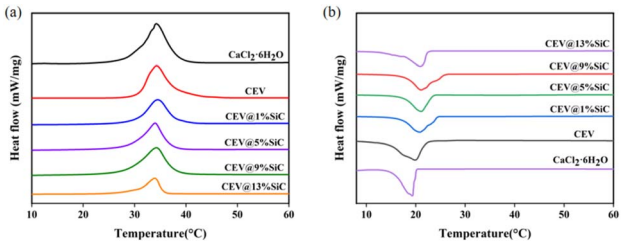

Fig. 5 DSC curves of the composites. (a) Melting and (b) crystallization curves of $CaCl_2·6H_2O$, CEV, and CEV@SiC composites with varying SiC content (0–13 wt%).

stretching vibrations from crystalline or adsorbed water.[18] The band at 1638.79 cm^{-1} is attributed to C=O stretching or aromatic C=C vibrations, and the sharp peak at 1030.34 cm^{-1} is associated with asymmetric stretching of Si–O–Si bonds. The characteristic Si–C vibration of pure SiC at 848.67 cm^{-1} remains clearly visible in the composite, indicating that the addition of SiC nanoparticles did not significantly alter the chemical structure of the matrix. Furthermore, the preservation of C–H stretching vibrations (2845–2952 cm^{-1}) from CEV and metal–oxygen vibrations (400–600 cm^{-1}) from $CaCl_2·6H_2O$ suggests that the components are combined through physical interactions without chemical recombination.[33]

Fig. 4b shows the X-ray diffraction (XRD) patterns of the individual components and the CEV@5% SiC composite. For pure $CaCl_2·6H_2O$, the characteristic diffraction peaks at 2θ = 13.01°, 22.61°, 26.03°, 32.03°, 39.62°, and 41.81° can be indexed to the (100), (110), (101), (111), (300), and (211) crystal planes, respectively, matching well with the standard pattern of $CaCl_2·6H_2O$ (JCPDS no. 26-1053). The expanded vermiculite (EV) matrix displays a broad, low-intensity peak around 2θ = 8–9° and another around 26–28°, which are characteristic of its layered silicate structure, indicating a predominantly amorphous or poorly crystalline nature. Pure SiC nanoparticles show sharp peaks at 2θ = 35.64° and 60.01°, corresponding to the (111) and (220) planes of its cubic β-phase (JCPDS no. 29-1129).

The XRD pattern of the final CEV@5% SiC composite retains all the characteristic peaks of $CaCl_2·6H_2O$ and β-SiC, while also showing the broad feature of the EV matrix. No new diffraction peaks are observed, and there is no detectable shift in the peak positions of the constituent phases. These results confirm that: (1) the crystalline integrity of $CaCl_2·6H_2O$ and SiC is preserved during the composite preparation process, and (2) the components are combined through physical interaction without any chemical reaction, successfully forming a ternary composite phase change material.

3.3 Thermal properties characterization of CEV and CEV@5% SiC composite PCM

Fig. 5a and b present the DSC thermograms of CEV composite phase change materials with varying SiC doping ratios, along with that of pure $CaCl_2·6H_2O$. Analysis of the melting and crystallization behaviors indicates that all samples exhibit characteristic phase change peaks, with the melting enthalpy (ΔH_m) of pure $CaCl_2·6H_2O$ serving as the reference. As the SiC content increases from 0% to 13%, the melting enthalpy of the composites initially rises and then decreases, as summarized in Table 1. The ΔH_m reaches a maximum for CEV@5% SiC, suggesting that an appropriate amount of SiC enhances thermal conductivity and interfacial adhesion, thereby improving crystallization efficiency. However, when the SiC content exceeds 5% (*e.g.*, 9% and 13%), ΔH_m decreases significantly, which is attributed to phase separation and pore blockage caused by excessive SiC, limiting the loading capacity of $CaCl_2·6H_2O$.

Table 1 Phase change enthalpy of composites with different SiC contents

Sample	ΔH_c (J g^{-1})	ΔH_c (J g^{-1})
$CaCl_2·6H_2O$	178.5	111.03
CEV	92.23	90.3
CEV@1% SiC	87.41	84.23
CEV@5% SiC	90.3	85.47
CEV@9% SiC	86.63	79.18
CEV@13% SiC	83.29	79.03

At a 5% SiC doping ratio, the composite exhibits high melting enthalpy, low supercooling, and excellent cycling stability. This performance enhancement arises from the synergistic interaction between SiC and the CEV matrix, which both reinforces the thermal conduction pathways and preserves the integrity of the porous structure. These findings provide critical experimental guidance for the compositional design of highly stable composite phase change materials.

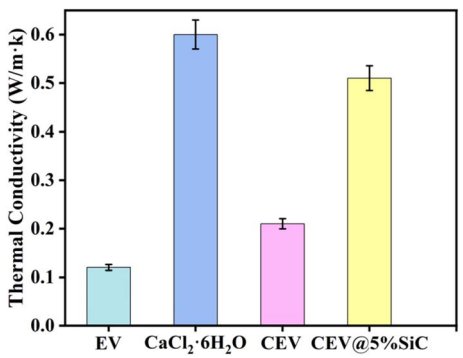

Fig. 6 Thermal conductivity of EV $CaCl_2·6H_2O$, CEV, and CEV@5% SiC.

Fig. 6 shows the thermal conductivities of expanded vermiculite (EV), calcium chloride hexahydrate ($CaCl_2 \cdot 6H_2O$), CEV ($CaCl_2 \cdot 6H_2O$/EV), and the CEV@5% SiC composite PCM. The thermal conductivity of EV is as low as 0.12 W (m^{-1} K^{-1}), which is attributed to its inherently poor heat conduction and the limited ability of EV alone to improve thermal transfer in composites. In contrast, the thermal conductivity of CEV@5% SiC is higher than that of EV, mainly because SiC possesses high thermal conductivity, which helps to reduce internal temperature gradients within the PCM, thereby minimizing heat loss and improving overall thermal management efficiency.

During the experiments, the temperature evolution of CEV and CEV@5% SiC was investigated. As shown in Fig. 7, both samples were placed on a heating plate maintained at 60 °C. CEV@5% SiC reached its phase transition temperature (29 °C) at 5 min and the peak temperature (60 °C) at 18 min, whereas CEV reached 29 °C at 8 min and 60 °C at 27 min. In both cases, the rate of temperature rise slowed significantly during the phase transition. However, CEV@5% SiC exhibited a faster heating rate than pure CEV due to the presence of SiC. This acceleration in temperature rise can be attributed to the improved thermal conductivity of the composite, which facilitated uniform heat distribution throughout the sample and prevented localized overheating that could cause material degradation.

Viewed together, the thermal conductivity and heating behavior demonstrate a balanced design of the CEV@5% SiC composite. The incorporation of SiC significantly enhances the thermal conductivity (compared to pure EV), establishing efficient heat transfer pathways to overcome the slow thermal response inherent to traditional shape-stable PCMs. Crucially, the resulting conductivity (~0.51 W (m^{-1} K^{-1})) remains considerably lower than that of metals and is comparable to that of the cement mortar matrix. This indicates that while acting as an efficient "thermal storage unit," the composite retains the necessary thermal insulation capacity required for building envelopes against ambient temperature swings. This combination of moderate thermal insulation and rapid thermal responsiveness is key to its function in dynamic thermal management.

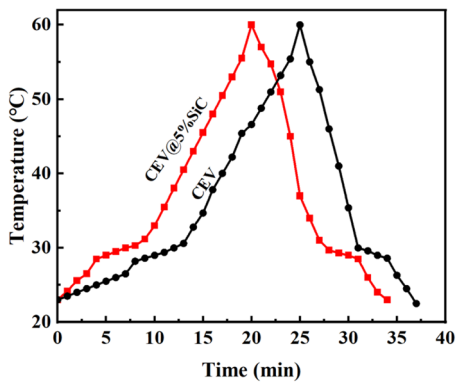

Fig. 7 Temperature variation curves of CEV and CEV@5% SiC.

3.4 Characterization of the phase change performances

To further investigate thermal stability, as shown in Fig. 8a, the temperature was increased from 20 °C to 60 °C over 15 minutes. By comparing the thermal stability results of $CaCl_2 \cdot 6H_2O$ and CEV@5% SiC, the following conclusions can be drawn: $CaCl_2 \cdot 6H_2O$ begins melting at its melting point (29 °C) after 3 minutes and is completely liquefied by 15 minutes at 60 °C. In contrast, the CEV@5% SiC composite phase change material remains stable under the same conditions, showing no melting within 15 minutes, demonstrating a significant thermal stability advantage. These results indicate that the CEV@5% SiC composite prepared in this study exhibits higher thermal stability and enhanced anti-leakage performance compared to pure $CaCl_2 \cdot 6H_2O$.

To investigate the heat storage capacity and buffering performance of $CaCl_2 \cdot 6H_2O$ and CEV@5% SiC, an infrared thermography experiment was conducted. Leakage of the phase change material from $CaCl_2 \cdot 6H_2O$ during heating was directly observed, as shown in Fig. 8b. During the gradual temperature increase, no significant difference in buffering capacity or heat storage ability was observed between the two samples below 30 °C. As the temperature continued to rise, $CaCl_2 \cdot 6H_2O$ melted, resulting in a substantial decrease in both its buffering capacity and heat storage ability. In contrast, the buffering capacity and heat storage ability of CEV@5% SiC continued to increase significantly. Comparison reveals that CEV@5% SiC demonstrates a notable improvement in both buffering capacity and heat storage performance, with only minimal leakage observed.

Fig. 9a presents the thermogravimetric (TGA) curves of EV, $CaCl_2 \cdot 6H_2O$, and the CEV@5% SiC composite PCM. EV shows negligible decomposition from room temperature to 600 °C.[34] In contrast, $CaCl_2 \cdot 6H_2O$ begins decomposing at around 29 °C, followed by three distinct stages of water loss at 137.7 °C, 163.7 °

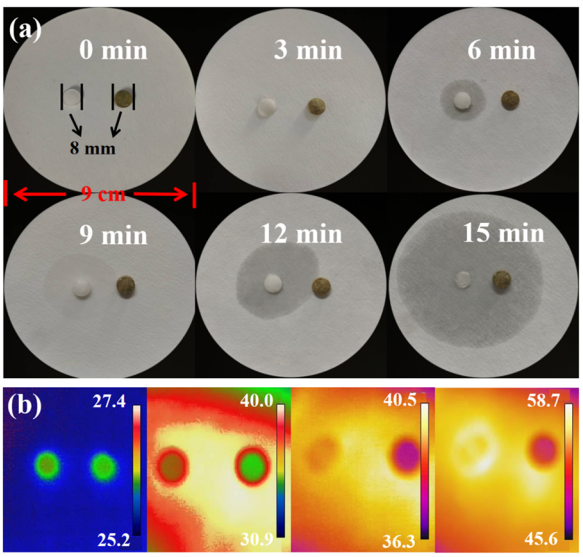

Fig. 8 (a) Photographs showing the leakage behavior of $CaCl_2 \cdot 6H_2O$ and CEV@5% SiC. (b) Infrared thermal images of $CaCl_2 \cdot 6H_2O$ and CEV@5% SiC.

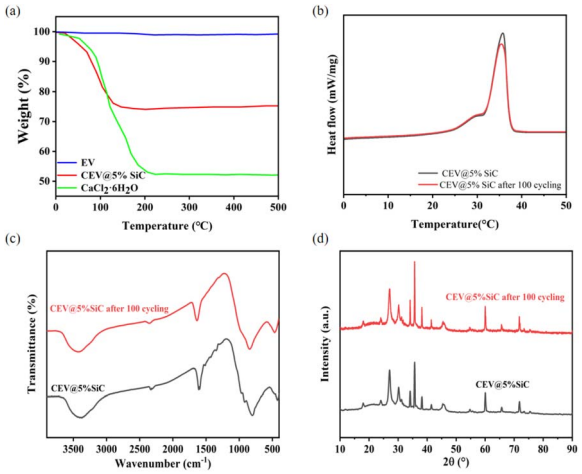

Fig. 9 Thermal stability and structural durability of the composite. (a) Thermogravimetric analysis curves of EV, $CaCl_2 \cdot 6H_2O$, and the CEV@5% SiC composite. (b–d) Characterization of the CEV@5% SiC composite before and after 100 thermal cycles: (b) DSC curves, (c) FTIR spectra, and (d) XRD patterns.

C, and 183.8 °C, with mass losses of 26.32%, 7.92%, and 11.89%, respectively. The total mass loss corresponds to 6.031 water molecules per formula unit, which is consistent with the theoretical value of 6. The CEV@5% SiC composite exhibits a similar dehydration process. The total water loss of the composite is 23.56%, which aligns well with the theoretical crystal water content (26.63%). After 100 thermal cycles (Fig. 9b), the melting enthalpy (ΔH_m) of the composite is 85.15 J g^{-1}, a decrease of only 3.3%, indicating minimal leakage of $CaCl_2 \cdot 6H_2O$. FTIR and XRD analyses (Fig. 9c and d) demonstrate the high structural stability of the composite after cycling. The FTIR spectra before and after cycling show high overlap between 3500 and 500 cm^{-1}, with no noticeable shift or reduction in characteristic peaks (*e.g.*, C–H, C=O, Si–O), confirming the integrity of chemical bonds and functional groups. The XRD patterns remain unchanged within the 20°–90° range, with no additional peaks, indicating excellent retention of the crystal structure, including phase composition and interplanar spacing. Overall, the DSC, FTIR, and XRD results confirm the exceptional cycling durability of the CEV@5% SiC composite, with no significant changes in chemical composition or crystalline structure after 100 cycles. The excellent retention rate (95%) over 100 thermal cycles demonstrates promising short-to-medium-term stability for the CEV@SiC composite. This 100-cycle test protocol is a well-established and widely adopted method for evaluating the medium-term stability of shape-stabilized phase change materials, as commonly practiced in related studies.[35,36] For building applications that require material performance over decades, long-term stability under thousands of cycles is indeed the ultimate benchmark. While accelerated testing over several hundred to thousands of cycles is recommended for comprehensive lifetime prediction, the minimal degradation observed in our 100-cycle test, coupled with the absence of structural or chemical changes (as confirmed by FTIR and XRD), provides a strong positive indicator of the material's inherent durability. This forms a solid basis for future long-term cyclic aging studies.

3.5 Thermal insulation test of the simulated unit house

The porous and lightweight structure of expanded vermiculite, combined with the surface reinforcement, water absorption control, and interfacial enhancement provided by the SiC coating, makes CEV@5% SiC a well-balanced material capable of effectively replacing conventional sand and gravel aggregates, and an excellent candidate for producing functional cement mortars with properties such as low density, thermal insulation, fire resistance, and sound absorption.

Based on the assumption that the cement mortar matrix is a homogeneous phase, a mesoscale model of phase change energy-storage mortar was constructed using a two-phase random composite approach, as shown in Fig. 10a. This model can be applied to calculate the effective thermal conductivity of the mortar and to analyze the internal heat transfer process. As illustrated in Fig. 10b, the incorporation of shape-stabilized PCM caused slight deflections in the isothermal lines within the mortar, indicating that the addition of PCM increases the conduction pathways of heat flow inside the energy-storage mortar.[37]

The CEV@5% SiC prepared in Section 2.2 was used to replace an equal mass of aggregate in the cement mortar and was mixed into the mortar, producing CEV@5% SiC composite cement mortar, as summarized in Table 2. A model house was then constructed using PVC panels, and its surfaces were plastered with either ordinary cement mortar or CEV@5% SiC composite mortar, resulting in a reference house and a phase change house.

Fig. 11 presents the monitoring results of indoor air temperature. It can be observed that the outdoor temperature during the day ranged from a minimum of 18.01 °C to a maximum of 35 °C. Regarding indoor conditions, the peak temperature in the phase change unit house was 2.04 °C lower than that in the reference house, and the occurrence of the indoor maximum temperature was delayed by 1 h. This effect can be explained by the fact that, during the daytime when the temperature exceeds the phase transition point, the PCM within the storage mortar melts and absorbs heat, thereby reducing heat transfer into the room and lowering the indoor peak temperature. At night, when the temperature drops below the phase transition point, the PCM solidifies and releases the heat

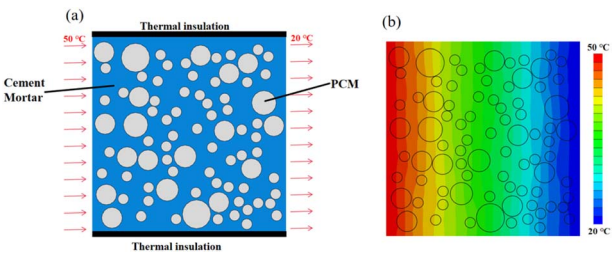

Fig. 10 (a) Mesoscopic and (b) heat transfer models of phase-change thermal storage mortar.

Table 2 Composite cement mortar mix proportions

Mortar mix proportion	PCM	Fine sand	Fly ash	Cement	Admixture	Water-cement ratio
Ordinary room						
Mass (kg)	0	799.7	75	125	0.3	0.5
Percentage (%)	0	79.97	7.5	12.5	0.03	0.5
Phase-change room						
Mass (kg)	100	699.7	75	125	0.3	0.5
Percentage (%)	10	69.97	7.5	12.5	0.03	0.5

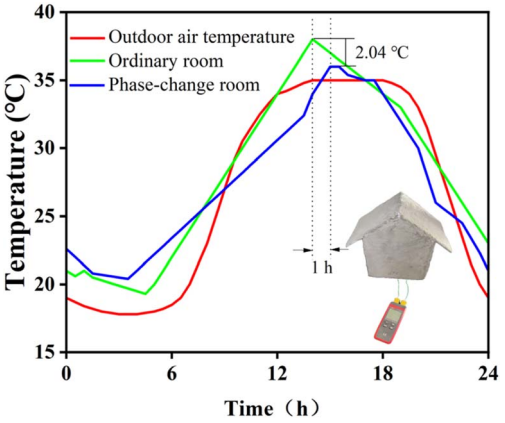

Fig. 11 24 hour indoor temperature variations in the ordinary room and phase-change room.

stored during the day, which helps to maintain a higher indoor temperature.

The magnitude of this peak temperature reduction (2.04 °C) represents a balanced outcome achieved under multiple practical constraints. This performance level can be attributed to three primary factors: (1) the PCM content within the mortar was limited to 10 wt% (as an aggregate replacement) to preserve the essential mechanical strength and workability of the construction material, highlighting the inherent trade-off between thermal storage capacity and structural integrity. (2) A thermal interface resistance exists between the cement matrix and the PCM composite, as indicated by the deflection of isothermal lines in the simulation (Fig. 10b), which implies that not all incident heat is uniformly absorbed by the PCM, allowing partial heat to bypass the storage mechanism. (3) The extreme climatic conditions of Northwest China, characterized by intense solar radiation and rapid diurnal temperature rise, posed a significant challenge by exceeding the instantaneous heat storage rate of the passive mortar system. These factors collectively define the current performance envelope and, more importantly, translate the experimental findings into clear motivations for future optimization—such as developing PCMs with better-matched phase-change temperatures, incorporating interfacial thermal enhancers, and integrating the phase-change mortar with other building envelope systems for synergistic effects.

This process effectively increases the thermal inertia of the wall assembly by adding a "capacitive thermal buffer," thereby delaying the arrival of the outdoor heat wave peak indoors. This phenomenon provides applied-performance evidence for the composite's thermal insulation capability. It demonstrates a synergistic effect where the material's dynamic heat storage complements the static insulation provided by the building envelope, collectively enhancing overall energy efficiency and thermal comfort.

3.6 Comprehensive evaluation of CEV@5% SiC

To objectively evaluate the application potential of the as-prepared CEV@5% SiC composite in thermal insulation and energy saving, a systematic performance comparison with representative composite PCMs reported in recent literature was conducted. The comparison focuses on three critical parameters for practical applications: the phase change temperature (T_m), the latent heat of fusion (ΔH_c), and the thermal conductivity (k). Key composite systems employing similar porous matrices (*e.g.*, expanded vermiculite, EV; expanded perlite, EP) for shape stabilization were selected as benchmarks. The comparative data are summarized in Table 3, which provides a clear overview of the performance landscape.

Based on the comparative analysis above, the CEV@5% SiC composite demonstrates well-balanced and competitive overall performance, making it suitable for thermal insulation and energy-saving applications. Although its latent heat of phase change is slightly lower than some reported systems, its phase transition temperature aligns more closely with the building thermal comfort range, and its thermal conductivity is significantly higher than that of similar porous matrix-based composite phase change materials. This combination of considerable heat storage capacity, suitable phase change temperature, and excellent heat transfer performance highlights its strong application potential in scenarios requiring efficient thermal buffering and rapid thermal response.

3.7 Outlook for energy-saving performance assessment

To translate the demonstrated thermoregulatory performance (Section 3.5) into directly quantifiable energy-saving indicators, we will construct structurally identical full-scale prototype rooms. Under real climatic conditions, by maintaining the same

Table 3 Comparison of thermal properties of CEV@5% SiC and reported PCMs for building applications

Material system	T_m (°C)	ΔH_c (J g^{-1})	Thermal conductivity (W (m^{-1} K^{-1}))	References
$Na_2SO_4 \cdot 10H_2O$–$Na_2CO_3 \cdot 10H_2O$/EV	23.98	110.3	0.192	38
$CaCl_2 \cdot 6H_2O$/EV	28.18	94.46	—	35
CA-PA/EV	23.61	67.5	0.25	39
$CaCl_2 \cdot 6H_2O$/EP	27.38	87.44	0.11	40
CEV@5% SiC	29	90.3	0.51	This work

indoor temperature-control settings and performing long-term monitoring of air-conditioning power consumption, direct energy-use comparisons will be conducted. This work aims to quantitatively evaluate the annual energy-saving efficiency of the phase-change mortar and to carry out a preliminary economic analysis, thereby providing a critical decision-making basis for its practical engineering applications.

4. Conclusions

A ternary composite phase change material (CEV@SiC) was successfully developed *via* vacuum impregnation for building thermal regulation. The optimized composite, with 50 wt% $CaCl_2 \cdot 6H_2O$ loaded into expanded vermiculite and enhanced by 5% SiC nanoparticles, exhibits a high latent heat of 90.3 J g^{-1} and excellent cyclic stability (95% retention after 100 cycles). Simulation and model-building tests demonstrated its effective thermal buffering capacity, reducing the indoor peak temperature by 2.04 °C and delaying it by one hour. This work provides a practical strategy for developing high-performance, shape-stable PCMs to improve energy efficiency in buildings under large diurnal temperature variations. Future work will focus on direct energy-consumption monitoring to bridge laboratory validation with practical application.

Author contributions

Chaoqun Fan: writing, methodology; Hanning Zhang: conceptualization; Jiaxing Gao: data curation; Yang Haiming: formal analysis; Xifeng Lv: supervision, funding acquisition.

Conflicts of interest

The authors declare that they have no known competing financial interests or personal relationships that could have appeared to influence the work reported in this paper.

Data availability

All data generated or analyzed during this study are included in this published article.

Acknowledgements

The authors acknowledge the assistance of Instrumental Analysis Center of Tarim University. Fund of State Key Laboratory of Organic–Inorganic Composites (oic-202401017), College Students' Innovation and Entrepreneurship Project (2025127) and First Division Science and Technology Program (2024GX10).

References

1 M. Sinka, D. Bajare, A. Jakovics, J. Ratnieks, S. Gendelis and J. Tihana, Experimental testing of phase change materials in a warm-summer humid continental climate, *Energy Build.*, 2019, **195**, 205–215.
2 Á. Lakatos, Novel Thermal Insulation Materials for Buildings, *Energies*, 2022, **15**, 6713.
3 H. M. Ali, T.-u. Rehman, M. Arıcı, Z. Said, B. Duraković, H. I. Mohammed, R. Kumar, M. K. Rathod, O. Buyukdagli and M. Teggar, Advances in thermal energy storage: Fundamentals and applications, *Prog. Energy Combust. Sci.*, 2024, **100**, 101109.
4 P. De Luca, I. Carbone and J. B. Nagy, Green building materials: a review of state of the art studies of innovative materials, *J. Green Build.*, 2017, **12**, 141–161.
5 R. Salman and S. Aljabair, "Energy storage technology: The growing role of phase change materials in the construction industry" a review, *Int. J. Thermofluids*, 2024, **23**, 100712.
6 Z. Yang, B. Liu and H. B. Zhao, Energy saving in building construction in China: A review, *Int. J. Green Energy*, 2004, **1**, 209–225.
7 S. R. L. da Cunha and J. L. B. de Aguiar, Phase change materials and energy efficiency of buildings: A review of knowledge, *J. Energy Storage*, 2020, **27**, 101083.
8 F. Hassan, F. Jamil, A. Hussain, H. M. Ali, M. M. Janjua, S. Khushnood, M. Farhan, K. Altaf, Z. Said and C. Li, Recent advancements in latent heat phase change materials and their applications for thermal energy storage and buildings: A state of the art review, *Sustain. Energy Technol. Assessments*, 2022, **49**, 101646.
9 X. Qi, Y. Zhang and Z. Jin, Building Energy Efficiency for Indoor Heating Temperature Set-Point: Mechanism and Case Study of Mid-Rise Apartment, *Buildings*, 2023, **11**(5), 1189.
10 J. Yan, H. Zhang, X. Liu, L. Ning and W. N. Hien, The Impact of Residential Cluster Layout on Building Energy Consumption and Carbon Emissions in Regions with Hot Summers and Cold Winters in China, *Sustainability*, 2023, **15**, 11915.
11 H. Mehling, Review of Classification of PCMs, with a Focus on the Search for New, Suitable PCM Candidates, *Energies*, 2024, **17**, 4455.

12 K. Yu, Y. Liu and Y. Yang, Review on form-stable inorganic hydrated salt phase change materials: Preparation, characterization and effect on the thermophysical properties, *Appl. Energy*, 2021, **292**, 116845.
13 X. Zhang, Y. Wang, Q. Huang and Y. Cui, Application and progress of latent heat storage technology, *Mod. Chem. Ind.*, 2017, **37**, 66–69.
14 Z. Chen, X. Zhang, J. Ji and Y. Lv, A review of the application of hydrated salt phase change materials in building temperature control, *J. Energy Storage*, 2022, **56**, 106157.
15 A. K. Hamzat, A. H. Pasanaje, M. I. Omisanya, A. Z. Sahin, A. O. Maselugbo, I. A. Adediran, L. O. Mudashiru, E. Asmatulu, O. R. Oyetunji and R. Asmatulu, Phase change materials in solar energy storage: Recent progress, environmental impact, challenges, and perspectives, *J. Energy Storage*, 2025, **114**, 115762.
16 A. M. Rashad, Vermiculite as a construction material - A short guide for Civil Engineer, *Constr. Build. Mater.*, 2016, **125**, 53–62.
17 A.-T. Abed and L. Eva, A comprehensive study of perlite in building materials: balancing sustainability and performance, *J. Therm. Anal. Calorim.*, 2025, **150**, 10627–10643.
18 J. Tian, J. Liu, X. Li, J. Song and L. Yang, Effect of carbon-based fillers on the thermal conductivity of polymers: A review, *Int. J. Heat Mass Transfer*, 2025, **253**, 127576.
19 T. S. Tie, K. H. Mo, U. J. Alengaram, S. K. Kaliyavaradhan and T.-C. Ling, Study on the use of lightweight expanded perlite and vermiculite aggregates in blended cement mortars, *Eur. J. Environ. Civil Eng.*, 2020, **26**(8), 3612–3631.
20 D. Jeon, W. S. Yum and J. E. Oh, Influence of expanded perlite and vermiculite pore structures on acoustic and thermal properties of quicklime-activated fly ash composites, *J. Build. Eng.*, 2025, **117**, 114728.
21 J. Balbuena, M. Sánchez, L. Sánchez and M. Cruz-Yusta, Lightweight Mortar Incorporating Expanded Perlite, Vermiculite, and Aerogel: A Study on the Thermal Behavior, *Materials*, 2024, **17**(3), 711.
22 X. Cui, J. Wang and G. Xia, Enhanced thermal conductivity of nanofluids by introducing Janus particles, *Nanoscale*, 2021, **14**(1), 99–107.
23 B. Abu-Jdayil, A.-H. Mourad, W. Hittini, M. Hassan and S. Hameedi, Traditional, state-of-the-art and renewable thermal building insulation materials: An overview, *Constr. Build. Mater.*, 2019, **214**, 709–735.
24 M. A. Raheem Junaidi, Influence of advanced composite phase change materials on thermal energy storage and thermal energy conversion, *J. Therm. Anal. Calorim.*, 2025, 1–22.
25 Z. Zhan, L. Lin, J. Zhang, Z. Li, Q. Zhang and Q. Wang, Effect of In Situ Polymerization on the Thermal Stability and Enthalpy Properties of Wood-Based Composites Based on Graphene Oxide–Modified Phase Change Microcapsule, *Polym. Compos.*, 2025, **46**, 15342–15356.
26 G. Xia, X. He, Y. Jia, Y. Zhu and Z. Tian, Design of a Cylindrical Thermal Rotary Concentrator Based on Transformation Thermodynamics, *Materials*, 2025, **18**(19), 4440.
27 X. Zhu, Z. Zuo, W. Wang, R. Liu and B. Jia, Design and single/multi-objective optimization of N-type Skutterudite/P-type half-Heusler-based thermoelectric modules based on an improved thermal resistance model, *Renewable Energy*, 2025, **250**, 123206.
28 Y. Yang, Y. Liu, Y. Chen, L. Wang and W. Feng, Bioinspired Stretchable Polymers for Dynamic Optical and Thermal Regulation, *Adv. Energy Sustain. Res.*, 2024, **5**(5), 2300289.
29 Y. Song, R. Xu, J. Hong, Y. Zhou, T. Shi, C. Wang and C. Xie, Preparation of a novel green lithium slag expansive agent: Enhancing deformation control, crack resistance, and durability of mortar, *Constr. Build. Mater.*, 2025, **495**, 143644.
30 M. Zheng, Y. Zhang, S. Yan, Z. Wu, X. Li, D. Wu and L. Xiong, Effect of carrier-encapsulated microbial calcium carbonate on the performance of cement mortar, *Constr. Build. Mater.*, 2025, **483**, 141579.
31 Z. Jiang, G. He, Y. Duan, Y. Jiang, Y. Lin, Y. Zhu and J. Wang, Contrasting effects of various factors upon the properties of foam ceramics and the mechanisms of crystalline phase reconstruction and microstructure regulation, *Ceram. Int.*, 2024, **50**, 21645–21657.
32 K. Ma, Y. Yu, B. Yang and J. Yang, Demand-Side Energy Management Considering Price Oscillations for Residential Building Heating and Ventilation Systems, *IEEE Trans. Ind. Inf.*, 2019, **15**(8), 4742–4752.
33 S. G. Zhang, X. L. Ma, X. Min, X. G. Zhang and J. H. Li, Expanded Vermiculite-Based Calcium Chloride Hexahydrate Phase Change Materials: Preparation, Characterization, and Phase Change Kinetics, *ChemistrySelect*, 2025, **10**(9), e202405355.
34 X. Lv, C. Fan, Y. Han, X. Tang, C. Zhang, D. Cai and H. Chen, Expanded vermiculite/D-mannitol as shape-stable phase change material for medium temperature heat storage, *Materials*, 2023, **16**, 6101.
35 H. C. Fan, Y. X. Li, Z. Zheng and T. W. Lan, Experimental study on preparation of composite phase change materials by expanded vermiculite with different particle sizes, *Non-Metallic Mines*, 2018, **41**(6), 63–66.
36 X. H. Li, S. Y. Liu, R. X. Bai, J. H. Zhang and J. N. Dai, Synthesis and Characterization of Capric Acid-Lauric Acid/Expanded Vermiculite as a Phase Change Composite for Energy Efficiency of Buildings, *J. Liaoning*, 2023, **43**(3), 34–40.
37 S. Li, B. Yu, M. Dong, Q. Jiang, Z. Dai, J. Huang and C. Wang, Experimental and theoretical studies on the freeze-thaw resistance of a phase change cement mortar, *Constr. Build. Mater.*, 2025, **486**, 141999.
38 N. Xie, J. Luo, Z. Li, Z. Huang, X. Gao, Y. Fang and Z. Zhang, Salt hydrate/expanded vermiculite composite as a form-stable phase change material for building energy storage, *Sol. Energy Mater. Sol. Cells*, 2019, **189**, 33–42.
39 R. Bai, S. Liu, J. Han, M. Wang, W. Gao, D. Wu and M. Zhou, Expanded vermiculite supported capric–palmitic acid composites for thermal energy storage, *RSC Adv.*, 2023, **13**(26), 17516–17525.
40 L. Fu, Q. Wang, R. Ye, X. Fang and Z. Zhang, A calcium chloride hexahydrate/expanded perlite composite with good heat storage and insulation properties for building energy conservation, *Renewable Energy*, 2017, **114**, 733–743.